Journal Name

ARTICLE

Effect of Azobenzene Derivatives on UV-Responsive Organic Thin-Film Transistors with a 2,7-dipentylbenzo[b]benzo[4,5] thieno[2,3-d]thiophene Semiconductor[†]

C.S. Smithson,[a)] D. Ljubic,[a)] Y. Wu,[*b)] and S. Zhu[*a)]

We have studied a UV responsive phototransistor and how the addition of various azobenzene derivatives alters the rise and relaxation times when exposed to and removed from UV light respectively. A three-component semiconductor system was studied consisting of a UV responsive material C5-BTBT, a polymer binder PMMA, and 1 of 5 different azobenzene materials for UV response enhancement. The highest occupied molecular orbital (HOMO) and lowest unoccupied molecular orbital (LUMO) were determined experimentally and found from DFT theory. Azobenzene units with a pendent nitro group have lower HOMO and LUMO levels than the semiconductor C5-BTBT. This combined with their electron withdrawing nature allow them to stabilize excited electrons, extending the lifetime of excitons, keeping the system at a high current longer. Using a bi-exponential model, we see the relaxation rate constant τ increase from 278 to 578 s when nitro-azobenzene was used. Meanwhile, when azobenzene contains the electron donating unit -NH₂, the HOMO of the material was found to be higher than that of C5-BTBT. This allowed another pathway for excited electrons to decay to their ground state, causing hole pair recombination, reducing I_{DS}. The relaxation curves when UV light is removed demonstrate a clear increase in decay rate over the control system, showing the charge donating amino-azobenzene assist in charge recombination.

Introduction

Organic Thin-Film Transistor (OTFT) technology offers many new opportunities for future electronic development.[1] One opportunity is the advanced functionality that can be applied to an OTFT by altering the semiconductor material, something that cannot be done for silicon based devices. Among the advanced OTFTs a need exists for easy to fabricate UV sensitive devices for a number of applications including ultraviolet sensing and memory. UV sensors can be generated from either a UV-diode, or UV-OTFT. In both devices, charge carrier density is altered by an incident UV light. In UV-OTFTs the drain current (I_{DS}) is increased by altering the gate voltage (V_{GS}) whereas, a UV-diode does not require a gate voltage for I_{DS} enhancment.[2,3] A major necessity for these devices to separate them from silicon based devices is the need for them to be blind to the visible spectrum. Current UV sensors require the use of inorganic materials such as Si, Cd, Ga Ge[4] and

ZnO[5,6,7,8] and often require waveguides to split the light allowing only UV light to enter the sensor.[9] The use of these waveguides complicates device structure (increasing costs), and reduces efficiency due to loss and a need to block the sensor from the original incoming UV light.

Photoswitching is one promising option where the response of the material to a photo stimuli dictates the device's switching speed. Gold nanoparticles have been used for this approach.[10] Another common way to utilize photoswitching is to generate a bistable device based on the OTFT design and incorporate photochromic materials such as spiropyran[11], or diarylethane[12,13,14] into the semiconductor. Typically these materials are mixed with a semiconducting polymer such as poly(3-hexylthiophene-2,5-diyl) (P3HT).[15] The devices function by altering the highest occupied molecular orbital (HOMO) of the photochromic material when photo stimulated so it more closely matches that of the semiconductor or work function of the electrodes.[16] Another approach for UV-OTFTs is to utilize a small molecule semiconductor that has a specific UV absorption such as BPTT, which absorbs at 380 nm with a photocurrent to dark current ratio of 2x10⁵.[17] For all the mentioned organic devices, if they can match inorganic device quality and sensitivity, the advantages associated with organic electronics can be gained including solution processability, potential device flexibility, and reduced manufacturing costs.

In this paper we investigate a photosensitive OTFT where an photon excites an electron to a higher energy state generating an exciton, which through the applied drain source voltage

a. *Department of Chemical Engineering, McMaster University, Hamilton, Ontario, LS8 4L8, Canada. E-mail: smithc62@mcmaster.ca, ljubicd@mcmaster.ca zhuship@mcmaster.ca*
b. *Xerox Research Centre of Canada, 2660 Speakman Drive, Mississauga, Ontario, L5K 2L1, Canada. Current address: Corporate Research, TE Connectivity, 306 Constitution Drive, Menlo Park, CA, USA, 94025. E-mail: yiliang.wu@te.com.*
† C.S. Smithson and D. Ljubic are visiting students at the Xerox Research Centre of Canada.
† Supplementary Information (ESI) available: [Detailed experimental conditions, optical microscopy images, duel sweep transfer curves, CV curves, UV-vis curves, rise and decay curves with fitting]. See DOI: 10.1039/x0xx00000x

(V_{DS}) allows for the generation of an electron-hole pair, increasing the devices conductivity.[18] It has been observed that the bulk of charge transport occurs at the semiconductor/dielectric interface, where we expect the generated holes to remain while the electrons accumulate at the drain.[19] Knowing this we have expanded upon our original report which demonstrated that the UV sensitive material 2,7-dipentylbenzo[b]benzo[4,5] thieno[2,3-d]thiophene (C5-BTBT), which has an absorption edge that begins at 367 nm and peaks at 353 nm, making it completely transparent to the visible spectrum exhibits this type of photoconductivity. C5-BTBT is an excellent semiconductor and has shown high mobility values when used in OTFTs. In addition, it is solution processable and air stable, making it an ideal candidate for electronic devices. When mixed with a polymer binder such as poly(methylmethacryate) (PMMA), consistent and well dispersed films are formed. From these films we were able to generate bottom-gate top-contact OTFTs using a silicon wafer as the gate with a 200 nm SiO_2 layer as the dielectric and Au as the source and drain. The 1:1 blend of C5-BTBT:PMMA forms a semiconductor film with a modest mobility that we measured to be approximately 0.1 $cm^2V^{-1}sec^{-1}$. This mobility can be increased by two orders of magnitude through advanced printing techniques or the use of other polymer binders to alter the morphology.[2,20] The most interesting feature of this device is that, when exposed to UV light, with no gate bias present and a drain source voltage of

-60 V, a slow 6 order of magnitude increase in current is observed (the "on state"), which can be returned to its low current "off state" state by pulsing the system with a gate voltage of -60 V.[21] This photoinduced conductance is the source of study in this paper to which we develop guidelines for how to decrease the device response time to UV stimulus and extend its "on state" lifetime for memory devices or decrease the "on state" lifetime for sensors.

Our previous work used a disperse red 1 (DR1)-methyl methacrylate copolymer as both a binding matrix and for device enhancement, allowing the device to reach maximum current faster and extending decay lifetime compared to when pure PMMA was used as the binding matrix. In order to screen numerous materials, we replaced the DR1-PMMA copolymer with PMMA and a series of azobenzene small molecules to determine which has the strongest effect on the device performance and why. This approach causes an overall decrease in device performance because we go from a two-component system to a three-component system where the phase separation in the films is more complicated. However, this is acceptable, because it eliminates the cumbersome step of synthesizing numerous copolymers, allowing for a much faster and wider screening of materials. The materials include azobenzene containing no substituents (**Azo-1**), azobenzene containing an electron donating amino group (**Azo-2**), azobenzene containing an electron accepting nitro group (**Azo-3**), an azobenzene material with both groups (**Azo-4**) and the **DR1** small molecule so the results could be compared to the previous work (see Fig. 1). In addition, density function theory (DFT) calculations were used in conjunction with cyclic

voltammetry and UV-vis measurements to estimate the highest occupied molecular orbital (HOMO) and lowest unoccupied molecular orbital (LUMO) energy levels of the materials both theoretically and experimentally. These measurements show that the placement of both the HOMO and LUMO directly influences the turn on time and decay rate of the systems. In addition we found that the choice of an electron withdrawing or electron donating substituent, influence the device performance.
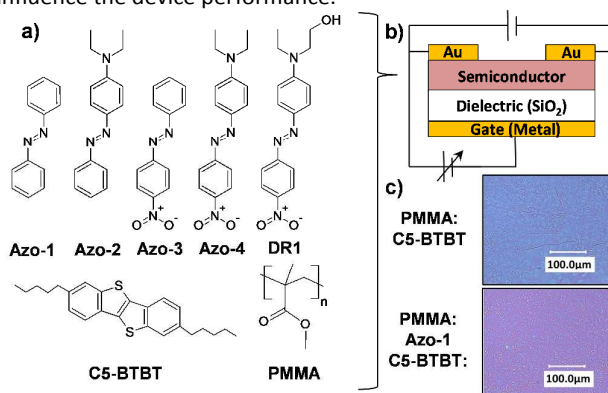

FIG. 1. *a)* Materials used to form the semiconductor layer. *b)* OTFT top contact bottom gate device design. *c)* Optical microscope images of a **PMMA:C5-BTBT** film and a **PMMA:Azo-1:C5-BTBT** film, showing that film morphology is not altered with the addition of the azobenzene small molecule.

Experimental / Results

All films were spin coated from a 1,1,2,2-tetrachloroethane (TCE) solution. TCE was chosen because it was able to completely dissolve all the materials used in this study to generate uniform films. The film morphology was not altered with the addition of azobenzene small molecules. When spin coated from the same solvent at the same conditions, films with different azobenzene additives also exhibited the similar morphology as shown in the optical images (Supporting Information Fig. S1). However, comparing the results of a C5-BTBT:PMMA film spin coated from chlorobenzene solution reported previously to films prepared from TCE, we observe different morphologies. Optical images of films made from TCE showed a large number of striations typical of polycrystalline domains (Fig. S1). The dispersion of these domains is very even but generates a significantly larger number of grain boundaries than films obtained from chlorobenzene solution. As a result, the device prepared from TCE showed a lower mobility and lower saturation current. The lower performance is acceptable because all films in this report are made from TCE; therefore they have the same morphology allowing comparisons among each other.

AFM measurements were performed to confirm the morphology was similar (Fig. 2). Topographical images show that all films have a relatively low surface roughness and are composed of small (~10 nm) spherical features evenly dispersed in the PMMA matrix. The phase images provide

more information, making it easy to distinguish between the small molecules and the polymer binder. **C5-BTBT** forms discrete spherical crystal domains within the film, with a large amount of overlap to form a percolating network. It appears

that the **C5-BTBT** domains are slightly bigger with less discrete edges when the polar azobenzene materials are present (**Azo-2**, **Azo-**
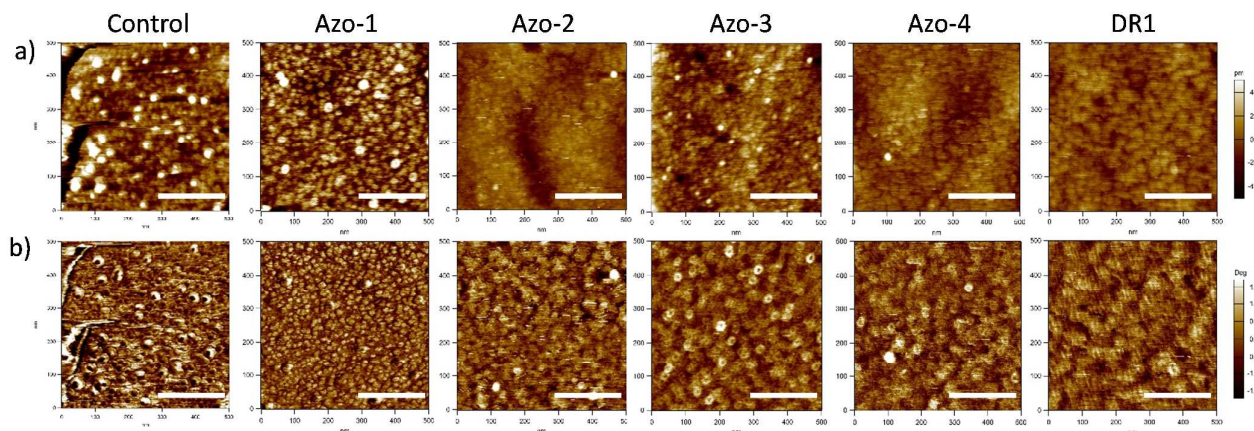

Fig 2. AFM images of the semiconductor films (scale bar 200 nm). (a) Topographical images, (b) phase image.

3, **Azo-4** and **DR1**), suggesting the polarity of the additive has an effect on **C5-BTBT** crystallization in the film. Unfortunately we cannot distinguish between the phase of the azobenzene additive and that of the semiconductor **C5-BTBT.**

Transfer curves in the dark demonstrate typical p-type behaviour for all samples (Fig. 3.). By considering the system containing no azobenzene small molecules (PMMA:C5-BTBT) as our control system, observations can be made as follows. Addition of azobenzene containing an amino group (**Azo-2**, **Azo-4**, **DR1**) shifted the threshold voltage (V_{Th}) towards the negative direction (Table 1) compared to the control. This is indicative of charge traps being introduced into the system.[22] Meanwhile, azobenzene samples that do not contain amine groups (**Azo-1**, **Azo-3**), showed a V_{Th} shift in the positive direction compared to the control to about -4 V, which suggests the filling of charge traps.[2] When the UV light was on, the V_{Th} of the control sample was shifted by only 14 V, while all the azobenzene containing samples showed much larger shifts, indicating the addition of the azobenzene small molecule allows for an increase in the number of charge carriers when exposed to UV light. It has been reported in the past that electrons generated by illumination fill the traps, causing the shift in threshold voltage.[23,22] The largest ΔV_{Th} occurs when a pendent amino group is present. The ΔV_{Th} can be used to estimate the increase in charge carrier density from dark to UV conditions, using the equation

$$\Delta N^* = C_i \Delta V_{Th}/e \quad [1]$$

where C_i = 15 nF cm^{-2} is the capacitance per unit area of the dielectric layer, ΔV_{Th} is the shift of the threshold voltage, and e is the elementary charge.[24,25,26] The photocurrent/dark-current ratio (P) was calculated at a V_{GS} = 0 V using equation **[2]**.

$$P = \frac{(I_{light} - I_{dark})}{I_{dark}} \quad [2]$$

where I_{light} and I_{dark} is the measured current under UV irradiation and in the dark respectively. These data are summarized in Table 1. A large photocurrent ratio eliminates

the need for additional circuitry to increase the device gain and can be used as a figure of merit for device performance. These devices exhibit a photocurrent/dark-current ratio between 3-6 orders of magnitude which is large enough to unambiguously
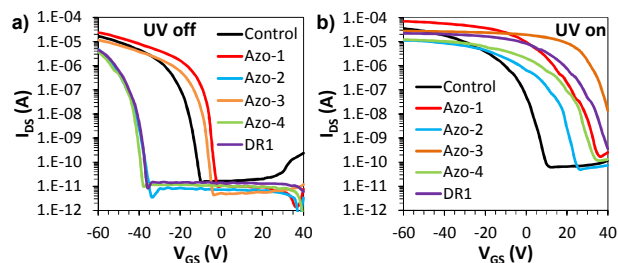

Fig. 3. Transfer Curves for the 6 systems studied with and without UV light. *(a)* From left to right Azo-4, DR1, Azo-2, PMMA, Azo-3, Azo-1. *(b)* From left to right PMMA, Azo-2, Azo-4, Azo-1, DR1, Azo-3.

Table 1. Electronic Characterization Data for the systems studied in dark and under UV light

Sample	P	Mobility dark (cm^{2}V^{-1} sec^{-1})	V_{Th} Dark (V)	V_{Th} UV on (V)	ΔV_{Th} (V)	ΔN^*
Control	3.3*10^3	0.10	-17	-3	14	1.87*10^{12}
Azo-1	9.2*10^5	0.08	-4	18	23	3.56*10^{12}
Azo-2	9.0*10^4	0.10	-43	12	55	5.62*10^{12}
Azo-3	3.7*10^6	0.04	-8	38	46	3.93*10^{12}
Azo-4	1.9*10^5	0.08	-42	23	65	6.74*10^{12}
DR1	5.8*10^5	0.10	-42	29	70	7.12*10^{12}

distinguish between the "off state" and "on state". Return sweeps for the transfer curves were measured, but make the graphs too cluttered. They can be found in the supporting information. It should be noted that in the dark, little to no hysteresis was observed. However, under UV irradiation, the

gate bias stress causes separated charges to recombine creating a large hysteresis effect.[27]

Similar to our previous report[21], all devices showed completely reversible behaviour. The devices were turned to their "on state" by applying a UV stimulus, while a large gate bias stress (V_{GS} = -60 V) returned them to their "off state". We were interested in how to speed up the rise times and alter the decay times for use as either a memory device (long decay time) or a sensor (short decay time). Fig. 4 provides the current response of devices over time when exposed to UV light for 20 minutes. All devices reached a saturation current within this period of time, the UV light was then removed and the decay of the I_{DS} was measured. The response and decay curves were fitted using biexponential models, one for the current rise when exposed to UV light **[3]** and one for the decay when the UV light was removed **[4]**.

$$I_{DS} = A\left(1 - e^{(-t/\tau_A)}\right) + B\left(1 - e^{(-t/\tau_B)}\right) + E \text{ [3]}$$
$$I_{DS} = Ce^{(-t/\tau_C)} + De^{(-t/\tau_D)} + F \text{ [4]}$$

where A, B, C, D, E and F are constants measured in (A), t is time in (s), τ_A and τ_B, are rise times given in (s), τ_C and τ_D, are decay times given in (s). The biexponential models consist of a fast
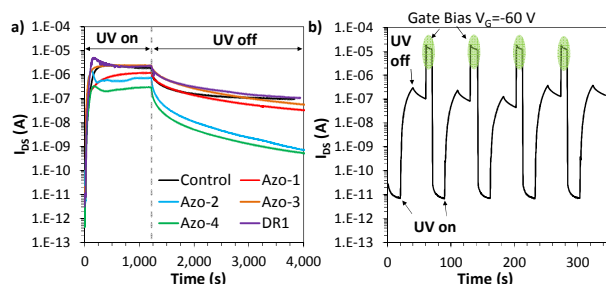

Fig. 4. (a) samples irradiated with UV light for 20 minutes to ensure saturation current, the dashed line shows when the UV is removed to show the current decay over time. (b) UV write erase cycle of Azo-3:PMMA:C5-BTBT showing the reproducibility and re-writability of the system.

Table 2. Values used to model the rise and decay curves of the samples.

	Writing (UV light exposure)				
	A (A)	τ_A (s)	B (A)	τ_B (s)	E
Control	$1.45*10^{-6}$	499	$9.00*10^{-7}$	$1.2*10^3$	$7.67*10^{-12}$
Azo-1	$1.20*10^{-6}$	371	$1.60*10^{-19}$	$6.7*10^3$	$1.21*10^{-11}$
Azo-2	$6.59*10^{-7}$	249	$8.05*10^{-8}$	$1.1*10^6$	$6.16*10^{-12}$
Azo-3	$2.40*10^{-6}$	125	$1.32*10^{-8}$	$1.4*10^5$	$7.67*10^{-12}$
Azo-4	$2.01*10^{-7}$	225	$2.20*10^{-6}$	$2.3*10^5$	$7.67*10^{-12}$
DR1	$2.01*10^{-6}$	306	$8.19*10^{-7}$	$2.8*10^3$	$7.67*10^{-12}$
	Decay (UV light removed)				
	C (A)	τ_C(s)	D (A)	τ_D (s)	E
PMMA	$1.02*10^{-6}$	18	$5.35*10^{-7}$	278	$1.10*10^{-7}$
Azo-1	$5.38*10^{-7}$	55	$4.58*10^{-7}$	516	$3.94*10^{-8}$
Azo-2	$6.93*10^{-7}$	50	$4.06*10^{-8}$	649	$9.00*10^{-11}$
Azo-3	$1.15*10^{-6}$	80	$8.48*10^{-7}$	578	$5.68*10^{-8}$
Azo-4	$2.70*10^{-7}$	47	$2.97*10^{-8}$	493	$4.37*10^{-10}$
DR1	$1.01*10^{-6}$	67	$7.85*10^{-7}$	580	$1.11*10^{-7}$

and slow exponential τ term. Table 2 summarizes the fitted values for each curve where the fast term was used as a measure of stimulus response speed and decay speed. For response times, devices containing nitro groups responded faster than the others. Those containing an amino group respond slower than pure azobenzene, likely due to the increased number of low energy traps generated from the amino groups. Over a 20 minute UV exposure, all the devices eventually reach a saturation value with azobenzene taking the longest of all the samples. There was a significant difference in the decay times of the devices. Devices containing electron accepting groups remained in the high current state, displaying slow decay times. Meanwhile the azobenzene containing electron donating groups (amino groups) displayed a significantly faster decay rate. Interestingly the DR1 sample does not follow the trend of the other amine containing groups, which could be caused by the additional electron withdrawal due to the OH pendent group on the amine unit.

HOMO LUMO energy level determination.

Given the very similar morphology of these systems, to understand the significant difference in photoresponse, we looked at the HOMO and LUMO energy levels of all materials involved in the charge transfer. DFT calculations using Gaussian 03 were performed using the B3LYP/6-311G(d,p) basis set to determine the energy levels of the HOMO and LUMO of each material. Hybrid functionals such as this one carry an average error of 0.2 eV. To provide an experimental comparison for the DFT calculations, cyclic voltammetry measurements were performed (Fig. 5.). Cyclic voltammetry measurements have been shown to be an excellent method to approximate the HOMO of a material. Varying viewpoints on how to analyze and standardize CV measurements exist in the literature,[28,29] making the comparison of HOMO and LUMO data difficult to achieve. Therefore, clearly stating the values used when converting CV measurements to the vacuum level is necessary for comparison with other works. We have chosen to follow the method set forth in 2011 by Cardona and Bazan,[30] which uses the onset of oxidation ($E_{onset, ox}$) obtained from cyclic voltammetry to determine the HOMO which is shown to have an accuracy of approximately 0.1 eV when compared to ultraviolet photoelectron spectroscopy (UPS) measurments.[28] To convert to the Fermi level the following equation is used;

$$E_{HOMO} = -(E_{[onset, ox vs Fc+/Fc]} + 5.1)(eV) \text{ [5]}$$

where the $E_{1/2}$ of the ferrocenium couple (Fc^+/Fc) in CH_3CN is given a value of 0.4 eV vs the saturated calomel electrode (SCE)[31] with SCE being 0.24 eV vs the normal hydrogen electrode (NHE) and NHE being -4.46 eV vs the vacuum level. Although it is possible to use $E_{onset, red}$ in the above equation to determine the LUMO value, a more accurate LUMO is obtained when the bandgap energy E_g is assumed to be equal to the $E_{onset\ opt}$ obtained from the optical edge of UV-vis measurements. This value is easily converted from nm to eV using the conversion;

$$E_{onset\ opt} = hc/\lambda = 1240(eV \cdot nm)/\lambda \text{ [6]}$$

where h is planks constant, c is the speed of light in a vacuum and λ the wavelength where the onset of absorbance occurs in the UV-Vis spectrum. The LUMO is determined using the following equation;

$$E_{LUMO} = E_{HOMO} + E_{onset\ opt}\textbf{[7]}$$

A general trend is observed, where the experimental HOMO-LUMO levels are found at a lower energy than the calculated values Fig. 5. This is expected as calculated values will always overestimate energy levels, and they do not take into account the solvent effect that occurs during CV measurements. However, the position of the HOMO and LUMO relative to one another is consistent across the experimental and calculated data, demonstrating that one or the other method can be used to obtain comparable HOMO/LUMO energy levels. To simplify, the rest of this report will focus on the experimental HOMO and LUMO levels. The HOMO of **Azo-1** and **Azo-3** are lower than that of the C5-BTBT. Meanwhile, all samples containing an amino group **Azo-2**, **Azo-4** and **DR1**, have a HOMO above that of C5-BTBT. The LUMO energy levels for all the materials are fairly close in energy with all of them being lower than that of C5-BTBT.

Charge transfer and trapping based upon HOMO LUMO energy levels.

The transistors studied here can be grouped into three different categories based on the relative positions of the azobenzene HOMO/LUMO energy levels compared to that of C5-BTBT. In the control system C5-BTBT:PMMA (Fig. 6. d), we observe that the HOMO of both materials are very close and because band theory assumes bands are not discreet energy levels, but instead a spread of the density of states, we can assume these two materials have overlapping HOMO levels. When irradiated with 365 nm UV light, an electron from the C5-BTBT valance band (HOMO) can be excited into the LUMO of the material leaving a hole in the valance band for conductance to occur. This hole is moved through the material due to the external V_{SD}, causing conductance to occur resulting in an increased current. While this is occurring, the electron can travel in the conductance band (LUMO) of C5-BTBT, but does not have the energy to enter the LUMO of PMMA as its LUMO lies higher in energy than the C5-BTBT LUMO, limiting the distance the electron can travel as it will eventually be stopped by PMMA. This excited electron will eventually return to its ground state causing a charge recombination.

When an azobenzene derivative is added to the system two new scenarios are generated (Figure 6. e, f). The second category occurs for both **Azo-1** and **Azo-3**, where the HOMO of the azo
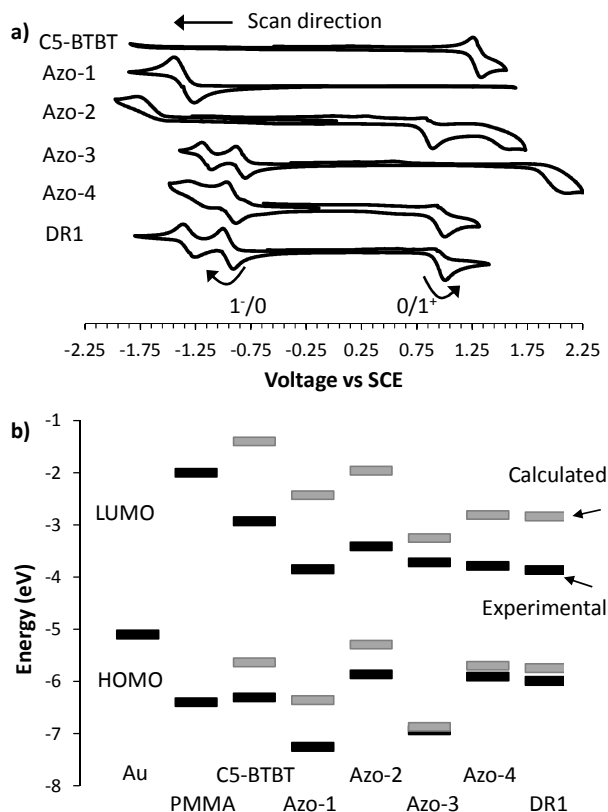

Fig. 5. *a)* Cyclic voltammetry measurements of the materials studied. The onset to oxidation (0/1$^+$) was used as the experimentally measured HOMO for each system. b) dark boxes, HOMO and LUMO energy levels measured from CV and UV vis, open boxes calculated using DFT theory with a B3LYP/6-311G(d,p) basis set. PMMA from the following reference[32]

Table 3. Cyclic Voltammetry and UV-Vis Data used to experimentally determine the HOMO and LUMO levels as well as the calculated HOMO and LUMO values.

Material	$E_{Onset\ Red}$ (eV)$^{a)}$	HOMO (eV)		$E_{opt\ onset}$ (nm)$^{d)}$	E_g (eV)		LUMO (eV)	
		Exper$^{b)}$	Calc$^{c)}$		Exper$^{e)}$	Calc$^{c)}$	Exper$^{f)}$	Calc$^{c)}$
C5-BTBT	1.21	-6.31	-5.63	367.1	3.38	4.23	-2.93	-1.40
Azo-1	-1.25 $^{g)}$	-7.25 $^{g)}$	-6.36	364.2	3.40	3.92	-3.85$^{g)}$	-2.43
Azo-2	0.76	-5.86	-5.29	505.5	2.45	3.33	-3.41	-1.96
Azo-3	1.84	-6.94	-6.87	384.8	3.22	3.62	-3.72	-3.25
Azo-4	0.81	-5.91	-5.70	583.5	2.13	2.89	-3.78	-2.81
DR1	0.89	-5.99	-5.74	583.7	2.12	2.91	-3.86	-2.84

$^{a)}$ Values determined from cyclic voltammetry vs SCE, scan rate 200 mV, solvent CH_3CN, electrolyte NBu_4PF_6, Pt electrodes
$^{b)}$ Values determined from cyclic voltammetry Vs Fermi level using equation [5]
$^{c)}$ Obtained using DFT with a B3LYP 6-311G(d,p) basis set;
$^{d)}$ Obtained from UV-vis
$^{e)}$ Using equation [6]
$^{f)}$ Obtained from equation [7]

g) only the oxidation peak was obtained from CV, so its onset was used as the LUMO and the UV-vis was used to determine the HOMO

is energetically unfavorable for the Azo unit to move an electron into a hole on C5-BTBT or PMMA and it therefore will not take part in hole conductance. The LUMO of these Azo systems is lower in energy than that of C5-BTBT. Therefore an excited electron on C5-BTBT can fall from the C5-BTBT conductance band into the LUMO of the Azo material. **Azo-3** has a strong electron withdrawing nitro group (which we see from the calculated molecular orbital, has a LUMO with a large electron concentration on the nitro group Fig. 6 b.) able to trap an excited electron for a longer time period than C5-BTBT. Because the HOMO of nitroazobenzene should not take part in hole transport, there is no lower energy Azo state for the electron to decay to. Therefore, as long as the Azo group retains the excited electron, hole conductance can occur. With time the excited electron will decay back to recombine with a hole on either C5-BTBT or PMMA. This dependence of the recombination of the excitons on the strength of the electron accepting material, provides a method to extend the hole lifetime after the UV source is removed

The final category occurs for the amino containing azobenzene systems (**Azo-2**, **Azo-4** and **DR1**) who's HOMOs are higher in energy than C5-BTBT and PMMA while their LUMOs are lower in energy than C5-BTBT. When UV light excites an electron on C5-BTBT, a ground state electron from the Azo HOMO can decay into the lower energy C5-BTBT HOMO filling the generated hole and placing the hole on the higher energy

amine-azobenzene HOMO. This is a trap which will prevent conductance because electrons will need to be raised in energy to fill this hole. Therefore enough excitons must first be generated to fill all the holes before conductance can occur. As a result it takes longer for a device to turn on. Like the previous scenario, the excited electrons can decay into the lower energy LUMO of the Azo group. It is possible the Azo system will already have donated an electron from its HOMO to fill the hole generated by C5-BTBT, therefore this excited electron can decay down to its electron deficient HOMO. Alternatively the electron can combine with a hole by decaying directly from the LUMO level to fill a hole in the C5-BTBT/PMMA conductance band. The calculated molecular orbital for the LUMO of these materials shows no molecular orbital density on the amino groups Fig. 6 c, supporting the idea that the material is more likely to donate an electron which can cause charge recombination. The result of this is an expected slower write time and increased decay rate.

Two other scenarios exits, but did not fall into the azobenzene systems studied here. Those systems are when the HOMO is lower than C5-BTBT and the LUMO is higher than C5-BTBT. This system is expected to have no appreciable effect on the systems performance, and will just take up physical space in the system generating gaps in the band structure. The other scenario is
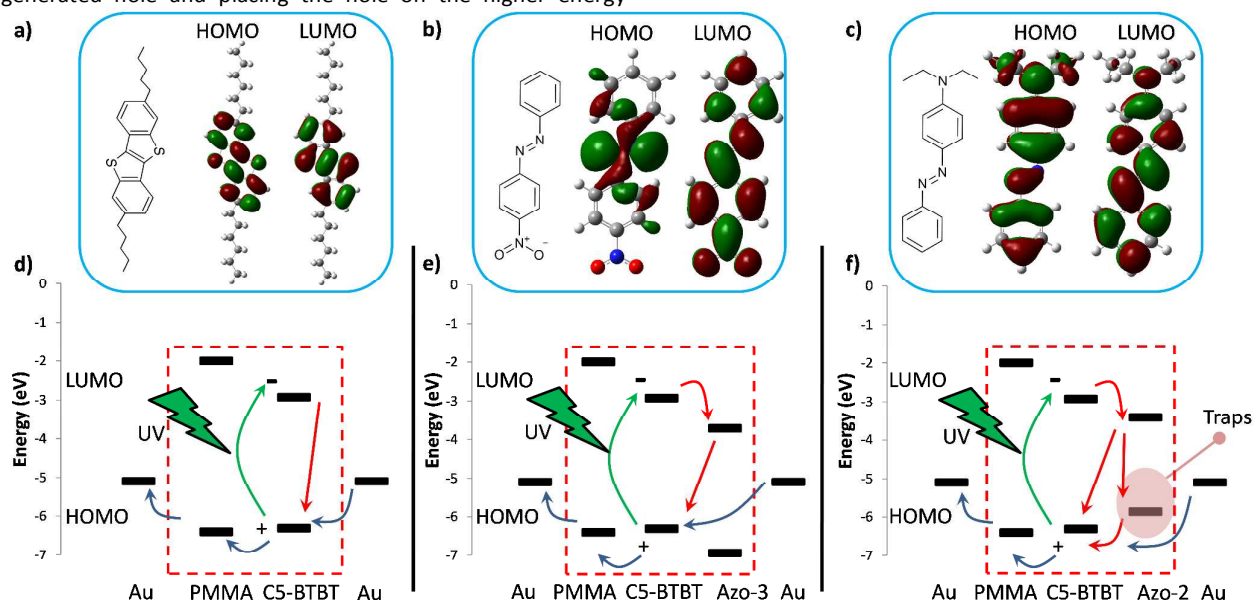

Fig. 6. The HOMO and LUMO molecular orbitals calculated using DFT theory for a) **C5-BTBT**, b) **Azo-3**, c) **Azo-2**. d),e),f) Experimentally determined HOMO LUMO energy levels of materials involved in charge transfer, explaining how each system reacts to the UV stimulus. The blue arrows represent pathways for electron movement to occur. The red arrow represents a pathway for charge recombination to occur.

when both the HOMO and LUMO are higher than those of C5-BTBT respectively. In this scenario, we expect a slower write time due to the traps caused by the material. The decay rate should also be faster because the traps provide a smaller bandgap where excited electrons can decay to and recombine.

Therefore this scenario would be similar to case three discussed   above. If we wish to generate a memory device we want to choose a material that has a HOMO lower than C5-BTBT and a LUMO lower than the C5-BTBT LUMO. Additionally the material

should contain a large amount of electron accepting groups so it can stabilize an excited electron for an extended period of time. Meanwhile if we want a sensor, we wish to choose a material that has a HOMO that matches C5-BTBT and a LUMO lower than C5-BTBT. The material should contain electron donating groups to help expedite the hole pair recombination process.

Conclusions

We explored the UV response of an OTFT consisting of C5-BTBT as a UV stimulant, PMMA as a polymer binder, and a series of azobenzene units containing different substituents. HOMO and LUMO energy levels were calculated and measured experimentally. Systems containing azobenzene with the electron donating amine groups, had HOMO values higher than that of C5-BTBT, which introduced charge traps into the system causing a slower response to the UV stimulus because the traps needed filling. In addition they had faster decay rates because the electron donating nature of the amine group combined with the charge traps provided an additional pathway for charge recombination to occur. Meanwhile, systems containing electron donating nitro groups were found have a much slower decay rate once the UV light was removed compared to systems without nitro groups because of the electron withdrawing nature of the nitro group, being able to stabilize an excited electron. These results provide a method to determine what materials can be mixed with C5-BTBT to enhance its UV response and either extend the decay time (memory device) (electron donating groups), or decrease the decay time (sensor device) (electron accepting groups). This roadmap can be used for future work to generate more effective UV devices.

Acknowledgements

Notes and references

1   H. Sirringhaus, *Adv. Mater.*, 2014, **26**, 1319–1335.
2   H. Yu, Z. Bao and J. H. Oh, *Adv. Funct. Mater.*, 2013, **23**, 629–639.
3   H. Hwang, H. Kim, S. Nam, D. D. C. Bradley, C.-S. Ha and Y. Kim, *Nanoscale*, 2011, **3**, 2275–2279.
4   M. Razeghi and A. Rogalski, *J. Appl. Phys.*, 1996, **79**, 7433–73.
5   N. N. Jandow, H. A. Hassan, F. K. Yam, K. Ibrahim and S. Gateva, in *Photodetectors*, 2009, pp. 3–32.
6   G. Chai, O. Lupan, L. Chow and H. Heinrich, *Sensor. Actuat. A-Phys.*, 2009, **150**, 184–187.
7   F. Zhang, Y. Ding, Y. Zhang, X. Zhang and Z. L. Wang, *ACS Nano*, 2012, **6**, 9229–9236.
8   S. N. Das, K. J. Moon, J. P. Kar, J. H. Choi, J. Xiong, T. Il Lee and J. M. Myoung, *Appl. Phys. Lett.*, 2010, **97**, 02213.
9   A. A. Chaaya, M. Bechelany, S. Balme and P. Miele, *J. Mater. Chem. A*, 2014, **2**, 20650–20658.
10   C. Raimondo, N. Crivillers, F. Reinders, F. Sander, M. Mayor and P. Samorì, *PNAS*, 2012, **109**, 12375–80.
11   S. Qian, G. Lin, L. Song, C. Yang, W. Zhen-Xing, H. Jing-Shu and G. Xue-Feng, *Acta. Phys-Chim. Sin*, 2010, **26**, 1941–1946.
12   E. Orgiu, N. Crivillers, M. Herder, L. Grubert, M. Pätzel, J. Frisch, E. Pavlica, D. T. Duong, G. Bratina, A. Salleo, N. Koch, S. Hecht and P. Samorì, *Nat. Chem.*, 2012, **4**, 675–9.
13   J. Frisch, M. Herder, P. Herrmann, G. Heimel, S. Hecht and N. Koch, *Appl. Phys. A*, 2013, **113**, 1–4.
14   M. El Gemayel, K. Börjesson, M. Herder, D. T. Duong, J. a. Hutchison, C. Ruzié, G. Schweicher, A. Salleo, Y. Geerts, S. Hecht, E. Orgiu and P. Samorì, *Nat. Commun.*, 2015, **6**, 6330.
15   J. Sayago, F. Rosei and C. Santato, *Nat. Photonics*, 2012, **6**, 639–640.
16   R. Hayakawa, K. Higashiguchi, K. Matsuda, T. Chikyow and Y. Wakayama, *ACS Appl. Mater. Interfaces*, 2013, **5**, 3625–30.
17   Y. Y. Noh, D. Y. Kim, Y. Yoshida, K. Yase, B. J. Jung, E. Lim and H. K. Shim, *Appl. Phys. Lett.*, 2005, **86**, 22–24.
18   X. Liu, Y. Guo, Y. Ma, H. Chen, Z. Mao, H. Wang, G. Yu and Y. Liu, *Adv. Mater.*, 2014, **26**, 3631–6.
19   A. J. Kronemeijer, V. Pecunia, D. Venkateshvaran, M. Nikolka, A. Sadhanala, J. Moriarty, M. Szumilo and H. Sirringhaus, *Adv. Mater.*, 2014, **26**, 728–733.
20   H. Ebata, T. Izawa, E. Miyazaki, K. Takimiya, M. Ikeda, H. Kuwabara and T. Yui, *J. Am. Chem. Soc.*, 2007, **129**, 15732–15733.
21   C. S. Smithson, Y. Wu, T. Wigglesworth and S. Zhu, *Adv. Mater.*, 2015, **27**, 228–233.
22   X. Wang, K. Wasapinyokul, W. De Tan, R. Rawcliffe, A. J. Campbell and D. D. C. Bradley, *J. Appl. Phys.*, 2010, **107**, 024509.
23   T. Pal, M. Arif and S. I. Khondaker, *Nanotechnology*, 2010, **21**, 325201.
24   C.-C. Chen, M.-Y. Chiu, J.-T. Sheu and K.-H. Wei, *Appl. Phys. Lett.*, 2008, **92**, 143105.
25   W. Wang, D. Ma and Q. Gao, *IEEE T. Electron Dev.*, 2012, **59**, 1510–1513.
26   G. Horowitz, *Adv. Mater.*, 1998, **10**, 365–377.
27   M. Egginger, S. Bauer, R. Schwödiauer, H. Neugebauer and N. S. Sariciftci, *Monatsh. Chem.*, 2009, **140**, 735–750.
28   T. Leijtens, I. Ding, T. Giovenzana, J. T. Bloking, M. D. Mcgehee and A. Sellinger, *ACS Nano*, 2012, **6**, 1455–1462.
29   P. I. Djurovich, E. I. Mayo, S. R. Forrest and M. E. Thompson, *Org Electron*, 2009, **10**, 515–520.
30   C. M. Cardona, W. Li, A. E. Kaifer, D. Stockdale and G. C. Bazan, *Adv. Mater.*, 2011, **23**, 2367–71.
31   N. G. Connelly and W. E. Geiger, *Chem Rev.*, 1996, **96**, 877–910.
32   Y. Zhang, X. Wang, Y. Liu, S. Song and D. Liu, *J. Mater. Chem.*, 2012, **22**, 11971.

Table of Content Color Graph
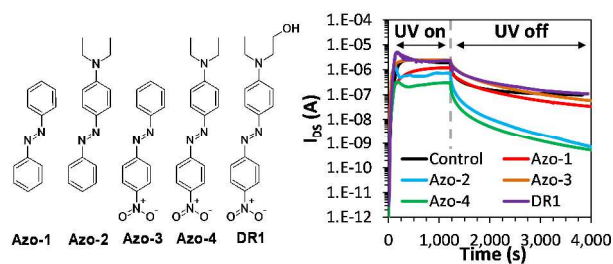
Text: Azobenzene derivatives with different substituents dramatically impact the photoresponsive behavior of organic thin-film transistors with a benzothiophene semiconductor.